Applied Physics Letters ARTICLE scitation.org/journal/apl

# Kinetics of environmentally assisted cracking in $SiN_x$ barrier films

Cite as: Appl. Phys. Lett. **115**, 051901 (2019); doi: 10.1063/1.5111400
Submitted: 25 May 2019 · Accepted: 9 July 2019 ·
Published Online: 31 July 2019

Hao Luo, Baolin Wang, Kyungjin Kim, Samuel Graham, Olivier N. Pierron,[a] and Ting Zhu[a]

## AFFILIATIONS

George W. Woodruff School of Mechanical Engineering, Georgia Institute of Technology, Atlanta, Georgia 30332, USA

[a]Authors to whom correspondence should be addressed: olivier.pierron@me.gatech.edu and ting.zhu@me.gatech.edu

## ABSTRACT

Kinetics of environmentally assisted subcritical cracking in $SiN_x$ barrier films is studied by *in situ* optical microscopy experiments and quantum chemical molecular orbital theory simulations. The activation volume of 0.83–1.11 $cm^3$/mol and the activation energy of 138 kJ/mol (1.43 eV) are experimentally measured for subcritical crack growth in moist air. The quantum chemical simulations reveal the molecular mechanism of stress corrosion in mechanically strained $SiN_x$ under water attack, and the predicted activation energy and activation volume are in good agreement with the experimental results. The combined experimental and modeling studies provide a fundamental understanding of subcritical crack growth in $SiN_x$ barrier films for flexible electronic device applications.

*Published under license by AIP Publishing.* https://doi.org/10.1063/1.5111400

Flexible electronic devices, such as solar cells, displays, and especially organic light emitting diodes (OLEDs), are constructed by mounting very thin active layers on flexible polymer substrates, such as polyimide or transparent conductive polyester films.[1] These devices are usually subjected to a variety of environmental and mechanical loading conditions. In particular, their active functional layers are highly sensitive to environmental attack from oxygen and water vapor. Hence, barrier films are necessary to protect these active layers from environmental attack. Recently, multilayer amorphous silicon nitride ($SiN_x$) thin films fabricated by plasma-enhanced chemical vapor deposition (PECVD) have found success in the development of flexible ultrabarrier coatings, as demonstrated for flexible displays.[33,34] Like other inorganic barrier layers, $SiN_x$ thin films are brittle and susceptible to mechanical failure.[2] For the application of $SiN_x$ as a mechanically reliable barrier layer, it is critical to characterize and understand the fracture in $SiN_x$ thin films on flexible substrates.

Previous studies indicate that stress-induced channel cracking is a primary failure mode in barrier layers, leading to subsequent device degradation.[3,29,32] These studies mainly reported the crack onset strain when long cracks appear in the barrier film on a polymer substrate during the bending or stretching test. However, the crack onset strain may not be sufficient to represent the failure resistance of a barrier film, since it does not account for time-dependent cracking that can be induced in flexible devices. Such subcritical cracking can be important for applications of bendable or foldable electronics that are held in a fixed state of strain for a period of time. Meanwhile, barrier films are expected to resist moisture and oxygen permeation. Therefore, understanding the coupling effects of mechanical loading and chemical attack is crucial for the application of barrier layers like $SiN_x$.[4–6]

We have recently studied time-dependent channel crack growth in PECVD $SiN_x$ barrier films deposited on polyethylene terephthalate (PET) substrates in different environments[7,8] and with substrate damage.[9] These studies revealed the occurrence of environmentally assisted subcritical cracking at strains well below the crack onset strain. Experimentally measured crack growth rates in laboratory air were an order of magnitude higher than those in inert environments, e.g., dry air and dry nitrogen, while the crack growth rates between dry air and dry nitrogen had no difference. These results indicated that water molecules are the chemically active species during environmentally assisted cracking in $SiN_x$ films.

Here, we combined experiment and molecular modeling to study the kinetics of environmentally assisted subcritical cracking in amorphous $SiN_x$ thin films on PET substrates. *In situ* optical microscopy experiments were performed to measure the rates of subcritical channel crack growth under different applied strains, environments, and temperatures. Semiempirical quantum chemical calculations based on the molecular orbital theory[21] and nudged elastic band (NEB) method[22,23] were performed to determine the reaction pathways of stress corrosion in mechanically strained $SiN_x$ clusters under water attack.[24,28] The activation energy and activation volume for subcritical crack growth in $SiN_x$ films were determined based on the experimentally measured crack velocities and further compared with molecular simulation results.


Published under license by AIP Publishing

The specimen for our subcritical cracking experiment was prepared by depositing a 250 nm $SiN_x$ film on a 125 $\mu$m PET substrate. The commercial heat-stabilized PET (Dupont Teijin Films Melinex ST505) was laser-cut to a size of 5 mm by 50 mm prior to deposition. Then, the amorphous $SiN_x$ film was deposited on the PET substrate using the Unaxis PECVD system with a radio frequency (rf) parallel plate configuration at a temperature of 110 °C, a pressure of 1 Torr, a 20 W rf plasma, and a rate of 10 nm/min. Our previous XPS characterization revealed a Si/N ratio of 0.81, consistent with the literature.[7]

All tensile tests were carried out with a microtensile testing stage (Linkam Scientific Instruments, TST350). *In situ* optical microscopy (Edmund Optics, 1312 M 59–365) was utilized to observe the time-dependent crack propagation during these tests. Detailed experimental information has been described in our previous work.[7,8,10] Here, the tensile tests were conducted in various environments, including dry nitrogen (i.e., 2 ppm) and air (i.e., relative humidity content of 30%). Two types of tests were performed. The first one was to measure the crack onset strain, $\varepsilon_c$, at which the crack started propagation. During each test, the observation area was kept at $644 \times 643\ \mu m^2$. The measured value of $\varepsilon_c$ was used to evaluate the fracture toughness $K_c$ of the $SiN_x$ film. The other type of test was performed to measure the crack growth rate as a function of applied strain in different environments. The experimental setup is illustrated in Fig. 1(a). The specimen was kept at an applied strain below $\varepsilon_c$ and *in situ* optical microscopy was used to observe crack growth behaviors. Data of the crack length vs time were collected only for channel cracks with the neighboring crack spacing more than $\sim$40 $\mu$m. This ensures a negligible influence of neighboring channel cracks on the calculated stress intensity factor $K$ based on a single channel crack solution.[7] The crack growth rate at a given $K$ load was calculated by averaging over 20 cracks. As the film-substrate system was subjected to a fixed strain, the measurements of crack length vs time were made within a maximum of 30 min to prevent substrate cracking and appreciable changes in $K$.[7] The activation energy for subcritical crack growth was also determined by measuring the crack velocity at three different temperatures (25, 55, and 85 °C) under the same applied stress intensity factor $K$ of 1.07 MPa m$^{1/2}$, which is calculated from the crack energy release rate $G$ of 8.65 J m$^2$ by[11]

$$K = \sqrt{GY_f^*}, \quad (1)$$

where $Y_f^*$ is the plane strain elastic modulus of the film ($Y_f^* = 131$ GPa, assumed to be constant between 25 and 85 °C). The relationship between the crack driving force $G$ and applied strain $\varepsilon_{app}$ for a channel crack in the film-substrate system is given by[12,13]

$$G = ZY_f^*(\varepsilon_{app} + \varepsilon_{res})^2 h_f, \quad (2)$$

where $\varepsilon_{res}$ is the residual strain in the film, $Z$ is the dimensionless energy release rate that depends on the elastic mismatch between the film and the substrate, and $h_f$ is the film thickness.[14] The effect of temperature (from 25 to 85 °C) on the elastic moduli and therefore $Z$ was found to be negligible (from $Z = 11.8$ at 25 °C to 11.4 at 85 °C, based on a decrease in the measured elastic modulus of the substrate from 4.3 to 4.1 GPa). The main effect of temperature on $G$ arises from the changes in residual strain $\varepsilon_{res}$. The residual compressive strain in our PECVD $SiN_x$ films grown on PET was previously measured to be $\varepsilon_{res} = -0.15\% \pm 0.02\%$. Based on a mismatch of coefficients of thermal expansion between $SiN_x$ (1.5 ppm/K) and PET (19 ppm/K), $\varepsilon_{res}$ is expected to be −0.1% at 55 °C, −0.04% at 85 °C, and 0% at 110 °C (which was experimentally confirmed — visible cracks at room temperature became nearly invisible at 110 °C). Therefore, based on Eqs. (1)–(2), applied strains of 0.6, 0.55, and 0.49% at 25, 55, and 85 °C, respectively, provided the approximately identical total strain load of 0.45% and therefore the same driving force $G$ for determination of the activation energy for subcritical crack growth in $SiN_x$ films.

Figure 1(b) shows the measured crack growth rates in $SiN_x$ films as a function of applied stress intensity factor $K$ in different environments (i.e., air and dry nitrogen) and temperatures (i.e., 25 °C and 85 °C), respectively. The vertical dashed lines indicate the fracture toughness $K_c$ at different temperatures and match values from other investigations on similar PECVD $SiN_x$ films.[31,35] Since the crack growth rate depends sensitively on the applied $K$ load, the measured crack velocities can be fitted to an empirical power law relation,

$$\frac{da}{dt} = v = AK^n, \quad (3)$$

where $a$ is the crack length, $v$ is the crack velocity, and $A$ and $n$ are the material and environment dependent coefficients. The fitting values of $n$ range from 17 to 28 and are consistent with the typical values for region I subcritical crack growth, where low-velocity crack growth is controlled by the rate of stress corrosion reaction at the crack tip.[15–17]

Several models have been previously developed to characterize the kinetics of subcritical crack growth in region I.[15–17] The most widely used model adopts an Arrhenius-type relationship,[18]

$$v = v_0 \exp\left(\frac{-E^* + bK}{RT}\right), \quad (4)$$

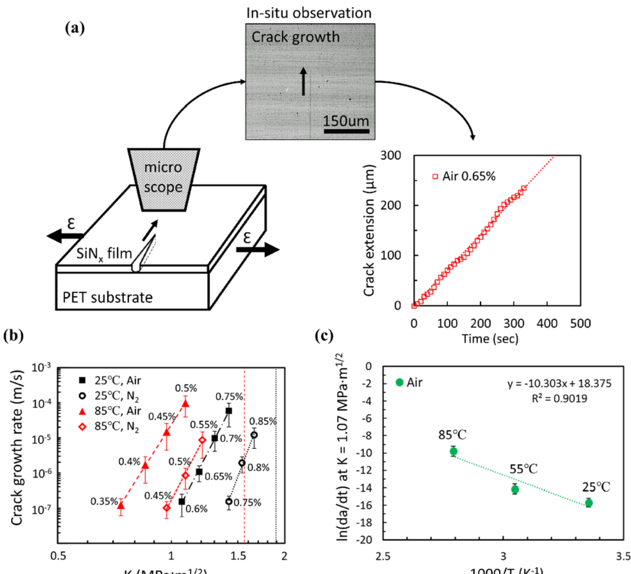


**FIG. 1.** *In situ* optical microscopy experiment of subcritical crack growth in a $SiN_x$/PET system. (a) Schematic illustration of *in situ* optical microscopy for the measurement of the crack length as a function of time. (b) Measured crack growth rate as a function of applied stress intensity factor $K$ at different temperatures for a channel crack in a 250 nm-thick $SiN_x$ film in air and nitrogen. (c) Dependence of the logarithmic crack growth rate on reciprocal temperature for a channel crack in a 250 nm-thick $SiN_x$ film in air.


Published under license by AIP Publishing

where $v_0$ is the velocity prefactor, $E^*$ is the so-called zero stress activation energy when $K = 0$, $R$ is the universal gas constant, $T$ is the absolute temperature, and $b$ is the constant that can be estimated by

$$b = 2V^*/\sqrt{\pi\rho}, \quad (5)$$

where $V^*$ is the activation volume for crack growth and $\rho$ is the radius of curvature of the crack tip. Fitting the measured data in Fig. 1(b) to Eq. (4) gives $b$ values for different testing conditions, which can be further used to calculate $V^*$ based on Eq. (5). Table I lists the fitted values of $b$ and $V^*$ for different environments and temperatures by taking $\rho$ as 0.5 nm (value also chosen by Wiederhorn *et al.*).[18] We compared the activation volumes for $SiN_x$ obtained in this study with the activation volumes for soda-lime-silica glass reported in the literature, considering that $SiO_2$ has a similar network structure to $SiN_x$ and also suffers stress corrosion by water that has been widely studied. Dauskardt *et al.* reported that the activation volume of soda-lime glass is 1.57 $cm^3$/mol in both moist air and dry $N_2$;[30] Wiederhorn *et al.* showed that the activation volume is 1.46 $cm^3$/mol in moist air.[18,19] These activation volumes for soda-lime glass are close to the corresponding results for $SiN_x$ obtained in this study.

The activation energy $E^*$ is another important parameter controlling the kinetics of crack growth and can also be experimentally determined. Figure 1(c) shows the crack growth rates as a function of reciprocal temperature at 25 °C, 55 °C, and 85 °C in the air environment and under the applied stress intensity factor $K$ of 1.07 MPa $m^{1/2}$. By combining Eq. (4) and a power law equation used to fit the data in Fig. 1(c), we obtained $E^* = 138$ kJ/mol by setting $b = 0.049$ $m^{5/2}$/mol.

To understand the molecular mechanisms that control the experimentally measured activation energies and activation volumes of subcritical crack growth in $SiN_x$ thin films, molecular modeling studies were performed to investigate stress corrosion in mechanically strained $SiN_x$ under water attack. We constructed two representative model systems, each of which consists of a hydrogen-passivated $\beta$-$Si_3N_4$ cluster with a nearby water molecule. The XPS spectra analysis of PECVD $SiN_x$ in our previous work[7] suggests that the structural units in $SiN_x$ films are similar to those in $\beta$-$Si_3N_4$. Hence, we constructed the cluster models based on the structural units of crystalline $\beta$-$Si_3N_4$ and used them to approximately represent the local atomic structures in amorphous $SiN_x$ films. Figures 2(a) and 3(a) show the atomic structure of the two model systems, respectively. One has a total of 93 atoms ($Si_{20}N_{24}H_{46}$ + $H_2O$, denoted as model I) and the other 95 atoms ($Si_{20}N_{26}H_{46}$ + $H_2O$, denoted as model II). The tensile strain was applied by a relative displacement between the two ends of the cluster, while the cluster was freely relaxed in its two transverse directions. In model I, the N—Si bond under the attack of an invasive water molecule is located at a Si—N—Si bridge within a small N—Si ring structure [Fig. 2(a)]. In model II, the

**TABLE I.** Coefficient $b$ and activation volume $V^*$ as a function of temperature and environment.

| Temperature | Environment | b ($m^{5/2}$/mol) | $V^*$ ($cm^3$/mol) |
|---|---|---|---|
| 85 °C | Air | 0.056 | 1.11 |
| 85 °C | $N_2$ | 0.056 | 1.11 |
| 25 °C | Air | 0.042 | 0.83 |
| 25 °C | $N_2$ | 0.046 | 0.91 |

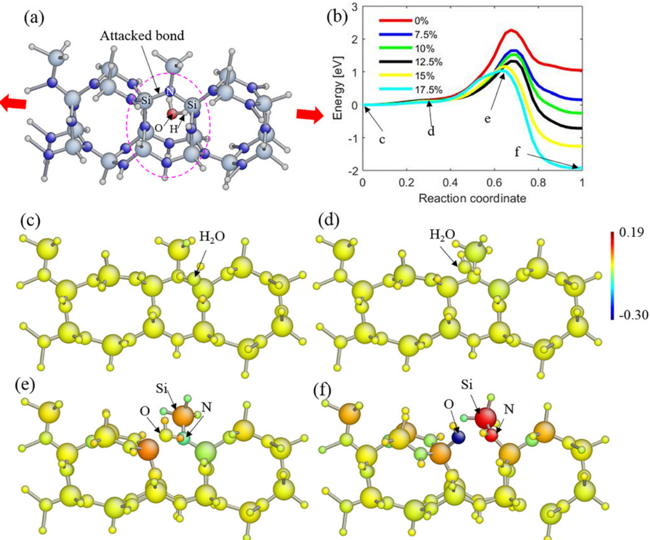


**FIG. 2.** Atomic structure of model I and stress corrosion simulation results. (a) Model I showing the water-attacked Si-N bond at a Si-N-Si bridge within a small Si-N ring structure (marked by a pink circle). The red arrows indicate the direction of applied tensile strain. (b) MEPs of the hydrolysis reaction at different applied tension strains. (c)–(f) Atomic configurations along the MEP under the applied strain of 17.5%, showing (c) initial state, (d) intermediate state, (e) saddle-point state, and (f) final state. Atoms are colored by the change of atomic charge relative to the initial state.

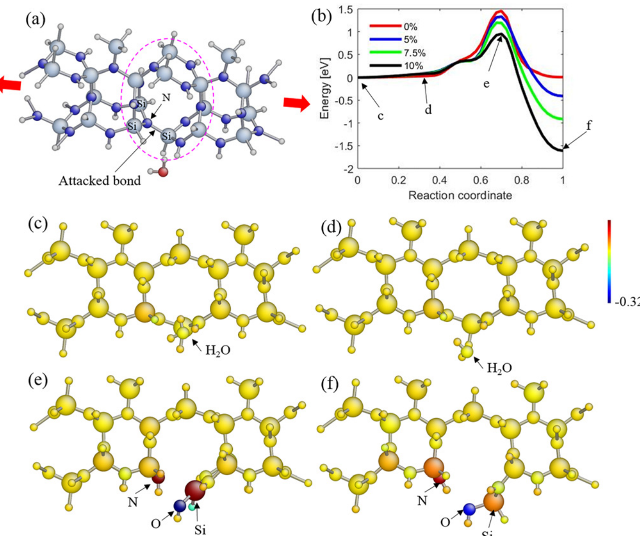


**FIG. 3.** Atomic structure of model II and stress corrosion simulation results. (a) Model II showing the water-attacked Si-N bond at a 2Si-N-Si bridge within a large Si-N ring structure (marked by a pink circle). The red arrows indicate the direction of applied tensile strain. (b) MEPs of the hydrolysis reaction at different applied tension strains. (c)–(f) Atomic configurations along the MEP under the applied strain of 10%, showing (c) initial state, (d) intermediate state, (e) saddle-point state, and (f) final state. Atoms are colored by the change of atomic charge relative to the initial state.


Published under license by AIP Publishing

N—Si bond under water attack is located at a 2Si—N—Si bridge within a large N-Si ring structure [Fig. 3(a)]. These N—Si bonds are aligned with the tensile loading direction and thus susceptible to mechanically assisted hydrolysis reaction with low activation energies.

Using the Molecular Orbital PACkage (MOPAC),[20] we calculated atomic bonding energies and forces in the two model systems based on molecular orbital theory using the AM1 method.[21] The reaction pathways and associated activation energies of hydrolysis reaction were determined at different applied tensile strains using the nudged elastic band (NEB) method.[22,23] To find the minimum energy path (MEP) of the hydrolysis reaction by the NEB method, we first determined the initial state (reactant) and final state (product), which correspond to two different local energy minima on the MEP. Note that a hydrolysis reaction usually occurs in two sequential steps:[24,28] physisorption of a water molecule to the cluster without any major bond breaking event, and chemisorption with the rupture of a Si-N bond and subsequent formation of new surface groups. We focused on chemisorption which is usually the rate-limiting step of the hydrolysis reaction.[24] For each NEB calculation under an applied tensile strain, a relaxed physisorbed structure was taken as the initial state and a relaxed chemisorbed structure as the final state. The former was obtained by placing a water molecule near the hydrogen-passivated $\beta$-$Si_3N_4$ cluster and then relaxing the system via energy minimization. Based on the previous studies of the hydrolysis reaction of $SiN_x$,[25–27] the latter was constructed by breaking the Si-N bond under water attack and then terminating the dangling bonds of Si and N with Si-OH and N-H groups; and this chemisorbed state was further relaxed by energy minimization. The NEB calculation was considered converged when the force on each replica is less than 0.05 eV/Å.

Figure 2 shows the NEB results of stress corrosion for model I. In Fig. 2(b), we plot the converged MEPs of the hydrolysis reaction at different applied tensile strains. For each MEP, the energy of the initial state is taken as zero, and the reaction coordinate $s$ is the normalized path length along the MEP between the initial state ($s = 0$) and final state ($s = 1$). For an applied tensile strain $\varepsilon^*$, the energy maximum on the MEP (i.e., the saddle-point state) gives the activation energy $E^a$ of the hydrolysis reaction. It is seen from Fig. 2(b) that $E^a$ decreases with increasing $\varepsilon^*$, which is consistent with the experimental results of increasing the stress corrosion rate with applied tensile loading. Note that $\varepsilon^*$ represents the local strain in the vicinity of the crack tip and thus is much larger than the macroscopically applied strain in experiment (<1%).[24] Figures 2(c)–2(f) show the cluster structures along the MEP when $\varepsilon^*$ is 17.5%, and the energy of each structure is marked in Fig. 2(b). Along the MEP, the initial state [Fig. 2(c)] corresponds to physisorption of a water molecule to the cluster; the saddle-point state [Fig. 2(e)] features rupture of a N-Si bond with the aid of an invasive water molecule; and the final state [Fig. 2(f)] shows termination of dangling bonds of N and Si by a proton and a hydroxyl group from the dissociated water molecule, respectively, resulting in the formation of surface Si-OH and N-H groups. In Figs. 2(c)–2(e), atoms are color-coded by the change of atomic charge (i.e., the Coulson charge calculated from MOPAC) relative to its initial value in Fig. 2(c). The atomic charges change drastically at the saddle-point state, indicative of substantial charge redistributions during the bond breaking and formation processes.

Figure 3 shows the NEB results of stress corrosion for model II, which are qualitatively similar to those in Fig. 2 for model I. However, at the same applied strain $\varepsilon^*$, the activation energy $E^a$ for model I is much higher than that for model II. For example, when $\varepsilon^*$ is 10%, $E^a$ values are 1.52 eV and 0.95 eV for model I and model II, respectively. To understand this difference, we note that in model I, the Si—N bond under water attack is within one of the three parallel Si—N—Si bridges that are aligned along the tensile loading direction and thus share the applied tensile load [Fig. 2(a)], while in model II, the Si—N bond under water attack is within one of the two parallel Si—N—Si bridges that share the applied tensile load [see Fig. 3(a)]. Hence, the water-attacked Si-N bond in model II is subjected to a higher load than that in model I and thus is more susceptible to the hydrolysis reaction with lower activation energy. Note that the zero stress activation energy $E^*$ defined in Eq. (4) corresponds to the NEB-calculated activation energy $E^a$ without applied strain ($\varepsilon^* = 0$), which is 2.27 eV for model I and 1.45 eV for model II. The latter is much closer to the experimentally measured $E^*$ value of 138 kJ/mol (=1.43 eV). Hence, the hydrolysis reaction in model II is considered as a closer representation of the stress corrosion process at the crack tip during experiment. This is further supported by the calculation of the activation volume from the two models. Based on the NEB results of $E^a$ vs $\varepsilon^*$, the activation volume $V^*$ can be calculated according to

$$V^* = -\frac{1}{Y}\frac{dE^a}{d\varepsilon^*}, \tag{6}$$

where $Y$ is Young's modulus (assumed to be 100 GPa). Following Eq. (6), we took the numerical derivative of $E^a$ with respect to $\varepsilon^*$ and obtained the activation volume $V^*$ of 6.8 $cm^3$/mol for model I and of 4.6 $cm^3$/mol for model II. These values are in good agreement with the experimental results. Since both the activation energy and the activation volume from model II are closer to the experimental results than model I, model II provides a better representation of the crack-tip stress corrosion process during experiment.

In summary, the kinetics of environmentally assisted subcritical cracking in $SiN_x$ barrier films was investigated experimentally by *in situ* optical microscopy. The experimental data of crack velocity were used to determine the activation volumes $V^*$ in the range of 0.83–1.11 $cm^3$/mol and the activation energy $E^*$ of 138 kJ/mol (=1.43 eV), which provide quantitative characterization of the kinetic parameters of subcritical crack growth in $SiN_x$ thin films in a water-containing environment. Semiempirical quantum chemical simulations were also conducted on two model systems to understand the molecular mechanism of stress corrosion in mechanically strained $SiN_x$. From a series of NEB calculations at different applied mechanical strains, we show that model II gives quantitative predictions closer to experimental values than model I, with the predicted activation volume of 4.6 $cm^3$/mol and the activation energy $E^*$ of 1.45 eV from model II. Our combined experimental and modeling studies provide a fundamental understanding of subcritical crack growth in $SiN_x$ barrier films. The results also provide a basis for further studies that integrate the controlled material processing, characterization, and modeling toward the enhanced resistance to environmentally assisted subcritical cracking in $SiN_x$ barrier films.

S.G., O.N.P., and T.Z. gratefully acknowledge support from NSF CMMI through Award No. 1400077.

## REFERENCES


[1] D. Shavit, Vac. Int. **1**, 35 (2007).

[2] K. Kim, X. Jia, C. Fuentes-Hernandez, B. Kippelen, S. Graham, and O. N. Pierron, ACS Appl. Nano Mater. **2**, 2525 (2019).




Published under license by AIP Publishing

[3]S.-H. Jen, J. A. Bertrand, and S. M. George, J. Appl. Phys. **109**(8), 084305 (2011).
[4]R. P. Birringer, R. Shaviv, P. R. Besser, and R. H. Dauskardt, Acta Mater. **60**(5), 2219 (2012).
[5]W. Vellinga, J. T. M. De Hosson, and P. Bouten, J. Appl. Phys. **112**(8), 083520 (2012).
[6]Q. Guan, J. Laven, P. C. Bouten, and G. de With, J. Appl. Phys. **113**(21), 213512 (2013).
[7]K. Kim, H. Luo, A. K. Singh, T. Zhu, S. Graham, and O. N. Pierron, ACS Appl. Mater. Interfaces **8**, 27169 (2016).
[8]K. Kim, S. Graham, and O. Pierron, Rev. Sci. Instrum. **88**(3), 036102 (2017).
[9]K. Kim, H. Luo, T. Zhu, O. N. Pierron, and S. Graham, Sci. Rep. **8**(1), 4560 (2018).
[10]K. Kim, O. N. Pierron, and S. Graham, J. Appl. Phys. **125**(4), 045301 (2019).
[11]T. L. Anderson, *Fracture Mechanics: Fundamentals and Applications* (CRC Press, 2017).
[12]J. W. Hutchinson and Z. Suo, Adv. Appl. Mech. **29**, 63 (1991).
[13]J. Beuth, Int. J. Solids Struct. **29**(13), 1657 (1992).
[14]J. Dundurs, J. Appl. Mech. **36**(3), 650 (1969).
[15]S. Wiederhorn and L. Bolz, J. Am. Ceram. Soc. **53**(10), 543 (1970).
[16]J. Rice, J. Mech. Phys. Solids **26**(2), 61 (1978).
[17]B. Lawn and T. R. Wilshaw, *Fracture of Brittle Solids* (Cambridge University Press, 1993).
[18]S. Wiederhorn, E. R. Fuller, and R. Thomson, Met. Sci. **14**(8-9), 450 (1980).
[19]S. M. Wiederhorn, S. W. Freiman, E. R. Fuller, and C. Simmons, J. Mater. Sci. **17**(12), 3460 (1982).
[20]J. J. Stewart, J. Comput.-Aided Mol. Des. **4**(1), 1 (1990).
[21]M. J. Dewar, E. G. Zoebisch, E. F. Healy, and J. J. Stewart, J. Am. Chem. Soc. **107**(13), 3902 (1985).
[22]H. Jónsson, G. Mills, and K. W. Jacobsen, *Classical and Quantum Dynamics in Condensed Phase Simulations* (World Scientific, 1998), p. 385.
[23]G. Henkelman and H. Jónsson, J. Chem. Phys. **113**(22), 9978 (2000).
[24]T. Zhu, J. Li, X. Lin, and S. Yip, J. Mech. Phys. Solids **53**(7), 1597 (2005).
[25]L. Bergström and E. Bostedt, Colloids Surf. **49**, 183 (1990).
[26]Y. Huang, J.-Q. Dai, Z.-P. Xie, T. Ma, J.-L. Yang, and J.-T. Ma, J. Eur. Ceram. Soc. **23**(6), 985 (2003).
[27]E. Laarz, B. V. Zhmud, and L. Bergström, J. Am. Ceram. Soc. **83**(10), 2394 (2000).
[28]T. A. Michalske and S. W. Freiman, Nature **295**(5849), 511 (1982).
[29]Y. Leterrier, Prog. Mater. Sci. **48**(1), 1 (2003).
[30]A. Bhatnagar, M. J. Hoffman, and R. H. Dauskardt, J. Am. Ceram. Soc. **83**(3), 585 (2000).
[31]K. Matoy, H. Schonherr, T. Detzel, T. Schoberl, R. Pippan, C. Motz, and G. Dehm, Thin Solid Films **518**(1), 247 (2009).
[32]A. Behrendt, J. Meyer, P. van de Weijer, T. Gahlmann, R. Heiderhoff, and T. Riedl, ACS Appl. Mater. Interfaces **8**(6), 4056 (2016).
[33]S. Zhang, W. Xue, and Z. Yu, Thin Solid Films **580**, 101 (2015).
[34]F. J. van Assche, S. Unnikrishnan, J. J. Michels, A. M. van Mol, P. van de Weijer, M. C. van de Sanden, and M. Creatore, Thin Solid Films **558**, 54 (2014).
[35]S. Jaddi, M. Coulombier, J. P. Raskin, and T. Pardoen, J. Mech. Phys. Solids **123**, 267 (2019).


Published under license by AIP Publishing